Analyst

Room-temperature formaldehyde sensor based on hematite for breast cancer diagnosis

Journal:	*Analyst*
Manuscript ID	AN-ART-11-2022-001796
Article Type:	Paper
Date Submitted by the Author:	01-Nov-2022
Complete List of Authors:	Zhang, Rui; Dalian University of Technology Liu, Chuanqun; Dalian University of Technology Wang, Pu; Dalian University of Technology Li, Yang; Norwegian University of Science and Technology Su, Yue; Institute of Semiconductors Chinese Academy of Sciences Dai, jianxun; Dalian University of Technology,

Analyst

Guidelines for Referees

Thank you very much for agreeing to review this manuscript for *Analyst*.

Analyst publishes analytical and bioanalytical research that reports premier fundamental discoveries and inventions, and the applications of those discoveries, unconfined by traditional discipline barriers.

Analyst's Impact Factor is **5.227** (2021 Journal Citation Reports®)

The following manuscript has been submitted for consideration as a

FULL PAPER

Original scientific work that has not been published previously. Full papers must represent a significant development in the particular field of analysis and are judged according to originality, quality of scientific content and contribution to existing knowledge. Although there is no page limit for full papers, appropriateness of length to content of new science will be taken into consideration. Further information on article types can be found on our website.

Please consider these standards when making your recommendation for publication in *Analyst*:

- Use the **journal scope and expectations** to assess the manuscript's suitability for publication in *Analyst*
- **Comment on** the originality, importance, impact and reliability of the science, with references as appropriate. Your comments should both help the Editor to make a decision on the article and the authors to improve it.
- English language and grammatical errors do not need to be discussed in detail, except where it impedes scientific understanding.
- All articles submitted to *Analyst* must meet the significant novelty criteria; routine and incremental work – however competently researched and reported – should not be recommended for publication.

Best regards,

Professor Norman Dovichi
Editor-in-Chief
University of Notre Dame, USA

Philippa Ross
Executive Editor
Royal Society of Chemistry

Contact us

Please visit our reviewer hub for further details of our processes, policies and reviewer responsibilities as well as guidance on how to review, or click the links below.

What to do when you review

Reviewer responsibilities

Process & policies

Highlights

- The morphologies of hematite nanocrystals are only influenced by reaction solvent.
- HCHO performance of the spindle hesitate stands out among the four hesitates.
- Comparison of adsorption energies and bond lengths support performance difference.
- Spindle hesitate differentiates healthy breath and simulated breast cancer breath.

Dear editorial board of ***Analyst***,

Here within enclosed is our paper for consideration to be published on "***Analyst***". The further information about the paper is in the following:

The Title: **Room-temperature formaldehyde sensor based on hematite for breast cancer diagnosis**

The Authors: Rui Zhang, Chuanqun Liu, Pu Wang, Yang Li, Yue Su, Jianxun Dai

The increased emissions of various pollutants that adversely impact air quality have been recognized as major environmental and health risks. The development of gas sensing materials to meet the demands for sensitive, rapid, and user-friendly sensors has become an important research direction for the assessment of environmental samples. Development of nanoscience and nanotechnology crucially depends on our ability to design and synthesize advanced nanomaterials. The cost-effective transition metal oxide semiconductors (TMOS) exhibited low activities and required an operation temperature of typically over 100 °C to achieve satisfied sensitivity and speed of HCHO sensing. When considering recent progress in materials science, it is recognized that TMOS with high-index exposed can provide excellent opportunities for sensing various gaseous targets. Consequently, as sensing materials in gas sensors, the hematite nanocrystals with (012)-facet exposed have a stable response/response behavior of less than 3 s and are able to retain its sensitivity through reproductivity of the device, i.e., 42, to 50 ppm HCHO gas at room temperature. Moreover, the experimental results coincide with theoretical calculations. This work highlighted that the facet engineering could be regarded as an efficient strategy for the gas device design.

We believe this article will be of great interest to a wide audience in "***Analyst***". And we look forward to receiving comments from the reviewers. If you have any queries, please don't hesitate to contact me at the address below.

Thank you and best regards.

Sincerely yours,

Dr. Jianxun Dai
School of Optoelectronic Engineering and Instrumentation Science,
Dalian University of Technology, China
Email: jianxundai@dlut.edu.cn

Journal Name

ARTICLE

Room-temperature formaldehyde sensor based on hematite for breast cancer diagnosis

Received 00th January 20xx,
Accepted 00th January 20xx

DOI: 10.1039/x0xx00000x

www.rsc.org/

Rui Zhang[1], Chuanqun Liu[1], Pu Wang[1], Yang Li[3], Yue Su[4], Jianxun Dai*[2]

Formaldehyde (HCHO) is regarded as one kind of indoor pollutants. Additionally, HCHO serves as a biomarker in the exhaled breath of breast cancer patients. Early warning and management are crucial for environment and human health. Thus, we have elaborately synthesized hematite (α-Fe_2O_3) employing a facet-engineering hydrothermal strategy by fine-tuned solvent composition, with special attention to the effect of different exposed surface on HCHO detection. The spindle like α-Fe_2O_3 nanocrystals with (012) facet exposed exhibited impressively higher response towards HCHO at room temperature than that of the disk-like α-Fe_2O_3 with mainly (001) facet exposed, partly due to the abundant vacancy oxygen and adsorbed oxygen of high-index facets of α-Fe_2O_3. More importantly, our experimental results coincide with theoretical calculations. Overall, the surface engineering strategy could be extended to a versatile approach for HCHO detection.

1. Introduction

Formaldehyde (HCHO) is a kind of colorless but toxic pollutants. It has been recognized as the most common of hydrocarbon volatile organic compounds (VOCs) in indoor polluted air.[1] Frequent exposure to HCHO atmosphere significantly increases the risk of disease, such as sneezing, coughing, emesis, asthma and even underlying death.[2] In the work atmosphere, the exposure limit of HCHO is restricted to 0.08 ppm by the World Health Organization (WHO) and 1 ppm by the National Institute for Occupational Safety and Health (NIOSH), respectively.[3] Furthermore, the concentration of HCHO from human breath could serve as the biomarker for breast cancer (0.3-0.6 ppm from a healthy person and 1.2 ppm from a patient).[4] Hence, the emphasis given to environmental and health protection results in imperious demands for advanced HCHO sensors.

Metal oxide semiconductors (MOSs) are widely used materials for HCHO sensing due to their satisfactory sensitivity, fast response to the targets, low cost and simplicity in operation.[5-7] Typically, hematite (α-Fe_2O_3), a typical n-type MOS with a corundum-type structure, holds rich opportunities for surface engineering, becoming an appealing substrate for HCHO sensing. Many works focused on the composition and structure control of α-Fe_2O_3, including heterojunction fabrication, surface modification and lattice doping, which are efficient to enhance the sensitivity, selectivity and sensing speed of MOSs to VOCs, including HCHO.[8,9] However, the high working temperature of α-Fe_2O_3-based sensor (most at 200-400 °C) brings extra energy consumption for heating the sensing film and monitoring the sensor's temperature, causing difficulties in miniaturization and integration. Additionally, the stability of sensing layers decreases with the growth of α-Fe_2O_3 grains that are induced by heating. Thus, it is always a challenge of HCHO sensing at relatively lower temperature or even ambient temperature.

The gas adsorption process strongly depends on the atom species, dangling bonds and the density of oxygen defects of the surface of sensing layer. Thus, endowing α-Fe_2O_3 with an exposed facet that was composed of high density of atomic steps could offer large amounts of coordinatively unsaturated active sites, resulting in higher catalytic activity and lower working temperature for gas adsorptions. For example, Deng *et al.* reported that Fe_2O_3 {113} facet interaction increased the density of active oxygen species, further boosting the activation of O_2 and NO.[10] Similarly, hollow α-Fe_2O_3 octadecahedrons enclosed by {113} and {104} facets were conducive to generation of O-vacancy and surface OH species, resulting in high activity and stability to HCHO.[11] However, there have been few studies and efforts in developing facet-enclosed α-Fe_2O_3-based HCHO gas sensing devices at room temperature.

Herein, a series of single-crystalline α-Fe_2O_3 nanocrystals (NCs) with disk (D), cylinder (C), ellipsoid (E) and spindle (S)-like morphologies were well-controlled and synthesized by hydrothermal method. The spindle-like NCs were enclosed with facets of high surface energy, and presented remarkable sensing ability to HCHO with a liner range from 1 to 10 ppm

1. School of Environmental Science and Technology, Key Laboratory of Industrial Ecology and Environmental Engineering (Ministry of Education), Dalian University of Technology, Dalian, 116024, China.
2. School of Optoelectronic Engineering and Instrumentation Science, Dalian University of Technology, Dalian, 116024, China. E-mail: jianxundai@dlut.edu.cn
3. Department of Electronic Systems, Norwegian University of Science and Technology, NO-7491, Trondheim, Norway.
4. Institute of Semiconductors, Chinese Academy of Sciences, Beijing, 100864, China.

and a fast response-recovery speed (< 3 s) at room temperature. We built a sensor that could effectively distinguish healthy breath and simulated breast cancer breath using HCHO as the biomarker. Furthermore, the corresponding sensing mechanisms were studied and discussed with theoretical simulations.

2. Experimental section

2.1. Chemical materials

Iron(III) nitrate nonahydrate ($Fe(NO_3)_3·9H_2O$, 98%), ethylene glycol (EG, $C_2H_6O_2$, 99%), and ammonia solution ($NH_3·H_2O$, 25%) were used as the starting chemicals without further purification. Moreover, deionized water (DI) and absolute alcohol (EtOH) were also used in this experiment.

2.2. Chemical synthesis

The α-Fe_2O_3 NCs were prepared according to the previous reported hydrothermal methods with a slight modification.[12] In this work, $Fe(NO)_3·9H_2O$ (0.8 mmol) was totally dissolved in EG. Then, $NH_3·H_2O$ was dropped into the above mixture under continuous stirring for 1 h. The obtained suspension was transferred into a 50 mL Teflon-lined autoclave, following hydrothermally treated at 200 °C for 30 h. The collected precipitates were centrifugated for four times with DI and EtOH (1:1, 10000 rpm, 10 min). Finally, the brick-red precipitate was obtained through calcination at 500 °C for 2 h (10 °C/min). Target products with different morphologies were tuned by introducing different ratios of EG and $NH_3·H_2O$ in the mixed solution, that is, 13/7 mL, 10/10 mL, 7/13 mL and 5/15 mL for disk (D), cylinder (C), ellipsoid (E) and spindle (S)-like α-Fe_2O_3 NCs, respectively.

2.3. Characterization

Field emission scanning electron microscopy (FESEM, JEOL JSM-7500F microscope) and transmission electron microscopy (TEM, Tecnai G220S-Twin microscope) images were used to investigate morphology of samples. Selected area electron diffraction (SAED) and energy-dispersive X-ray spectroscopy (EDS) data were measured using the above TEM microscopy that equipped a spectrometer. The crystal structure and composition of samples were examined by X-ray diffraction (XRD, CuKα radiation source (λ = 1.54059 Å)) on a Rigaku D/Max-2550 diffractometer with a scan range of 20-80°. X-ray photoelectron spectroscopy (XPS) was conducted on a PREVAC X-ray photoelectron spectroscopy system. Electrical measurements of the sensing devices were recorded by a CHI 650E potentiostat-galvanostat (CH Instruments Inc.).

2.4. Fabrication of gas sensor

To study the sensing performance of α-Fe_2O_3 NCs, the as-synthesized samples were integrated onto the interdigital electrodes. First, 10 mg of samples were added into the 10 mL of DI to form the uniformly dispersed suspension under continuously ultrasonication. Then, 100 μL of the above dispersed suspension was drop casted onto an alumina ceramics substrate that was patterned with five pairs of Ag-Pd interdigital electrodes (IEs), and the gap and finger width of each IEs are both 0.2 mm. To improve the adhesion of the sensing material on the substrate, the sensors were then heated at 55 °C for 10 min before testing.

2.5. Measurement of gas sensor

A certain concentration of gas analytes was obtained by a static liquid gas distribution method according to the previous works.[13,14] The electrical signals were monitored on a CHI 650E potentiostat-galvanostat using a two-electrode configuration with a constant bias voltage of 10 V. The response (S) of the device was defined as follows, $S = (I-I_0)/I_0$, where I_0 and I represent the initial current in ambient air and dynamic current in target gases, respectively. The response time (T_{res}) and recovery time (T_{recov}) are the time required for the sensor to achieve 90% of current change maximum. The relative humidity (RH) atmospheres were prepared using different saturated salt solutions in their equilibrium states.[15]

2.6. Collection of breath samples

The exhaled breath samples were collected from ten health volunteer after eating at least 2 h and rinsing the mouth before testing. The exhaled samples were collected by a gas collection bag (1 L, BKMAM, Hunan, China). Then, 1.2 ppm of HCHO was injected to prepare the simulated gas mixture. Before testing, the simulated gas mixture was dried by silica-gel drier.

2.7. Computational details

The density functional theory (DFT) calculations of gas adsorption on α-Fe_2O_3 NCs were conducted by CP2K using the Gaussian and Plane Waves (GPW) method. In this calculation, the energy cutoff was set as 600 Ry. Additionally, DZVP-MOLOPT-SR-GTH for each atom with a Goedecker-Teter-Hutter (GTH) pseudo potential was used to set molecularly optimized basis.[16] The DFT-D3 was employed to accommodate the weak forces that might be present. The geometry optimizations were updated with the L-BFGS algorithm. 1×10^{-6} Hartree and 0.001 Hartree/Bohr were the energy convergence for the self-consistent field (SCF) calculation and the largest force on atoms, respectively. The adsorption energy ΔE_{ad} was calculated as follows, $\Delta E_{ad} = E_{mol/surf} - (E_{mol} + E_{surf})$, where $E_{mol/surf}$, E_{mol} and E_{surf} are the energies of the surface with adsorbates, an isolated analyte gas molecule, and the clean facet surface, respectively.[17]

3. Results and Discussions

3.1. Structural and morphological characterization

Well-shaped NCs from disk to spindle were regulated by controlling the volume ratio of $NH_3·H_2O$ to EG. The shapes of the NCs gradually varied from nanodisk to nanospindle with the decreasing aspect ratio (Fig. 1). The average edge length (EL) and average apex to apex length (AL) of D-α-Fe_2O_3 NCs are about 90 nm and 245 nm, respectively. The TEM images (Fig. 1a1) further confirmed the quasi-circular shape from the top view. Fig. 1a2 showed the corresponding SAED pattern of a single nanodisk. The ordered reflecting spots indicated that the top facet of D-Fe_2O_3 is the (001) plane. The HRTEM image

in Fig. 1a3 showed the related crystalline structure from the red rectangle in Fig. 1a1. The entire surface of the NC was perfectly aligned by three sets of parallel lattice fringes with an angle of 120˚ between each other. The d-spacing of lattice fringe is visible and measured as 0.25 nm, that corresponds to the (110), (-120) and (-210) planes of hematite (JCPDS 33-0664). And it could be deduced that the surfaces of the disk exposed (001) planes, which is consistent with the previous report.[12] The inset of related fast-Fourier transform (FFT) pattern agreed with the result of SAED and the single crystalline nature of the nanodisk was further confirmed. The corresponding SAED patterns illustrated that all samples were in good crystalline structure (Fig. 1(a2-d2)). In addition, as shown in Fig. 1(a3-d3), the parallel lattice fringes changed and were different from the (001) facets, indicating that the decrease of EG ratios facilitated exposing facets with higher energy than (001).[18] Thus, the sensors based on C-α-Fe_2O_3, E-α-Fe_2O_3 and S-α-Fe_2O_3 NCs were expected to show better performance than those of D-α-Fe_2O_3-based one.

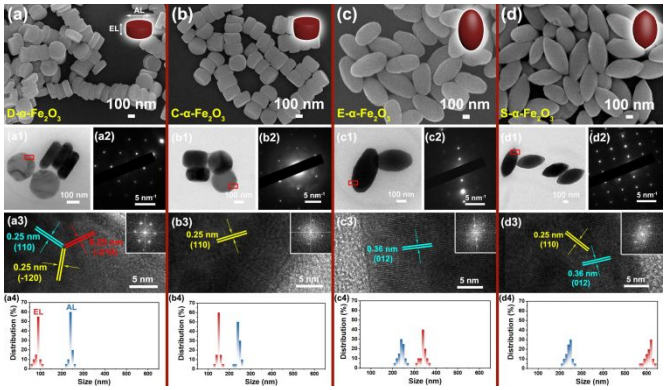

Fig. 1 SEM images of the as-synthesized α-Fe_2O_3 NC products: (a) D-α-Fe_2O_3, (b) C-α-Fe_2O_3, (c) E-α-Fe_2O_3, and (d) S-α-Fe_2O_3; (a1-d1) TEM images, (a2-d2) SAED patterns, (a3-d3) HRTEM images from the area of the red square in (a1-d1) and the related fast-Fourier transform pattern, (a4-d4) size distributions of four α-Fe_2O_3 samples.

With the decreasing ratios of EG to $NH_3 \cdot H_2O$, the surface of NCs became more irregular and rougher, implying that a facet with higher surface energy appeared.[18] The AL of all samples were 240-250 nm, but EL increased with the decreasing volume ratios of EG to $NH_3 \cdot H_2O$ (Fig. 1(a4-d4)). The EL-to-AL ratio of the NCs increased from around 0.4 to 2.5, which indicated that the tip growth was promoted. It could be speculated that the hindrance function to edge growth become stronger with the decreasing EG ratios, resulting in formation of ellipsoid and spindle-like particles.

High-index planes will be eliminated during the particle formation because of the minimization of surface energy. It is clearly observed that the morphology of α-Fe_2O_3 NCs changed from nanodisk to nanospindle, indicating that the <001> retarded growth became weaker. In this work, crystal anisotropy was only controlled through adjusting the mix ratio of EG to $NH_3 \cdot H_2O$. It is reasonable to assume that $NH_3 \cdot H_2O$ played a vital role in changing the growth rates of various facets of α-Fe_2O_3 NCs (Fig. 2a). Three types of surface hydroxyl groups (from $NH_3 \cdot H_2O$) with different coordination modes existed in α-Fe_2O_3 NCs, regarded as singly, doubly and triply coordination (donated as S, D and T). For (001), they were all inert D coordination. However, for other common crystal faces of α-Fe_2O_3, such as (100), (110) and (012), S and T-coordination exhibited, which were reactive. Thus, adsorption capacities and affinities of NH_3, which equipped with a lone pair of electrons, were much higher for (100), (110) and (012) planes than (001) plane, further retarding these crystal planes from taking part in further reactions growth (Fig. 2b).

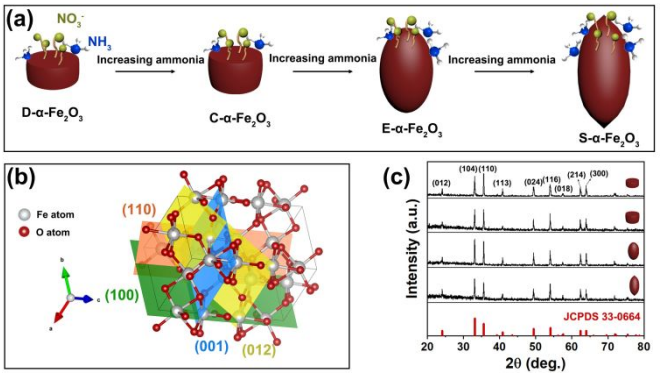

Fig. 2 (a) Schematic diagram of the evolution of morphology from D-α-Fe_2O_3 to S-α-Fe_2O_3; (b) Configuration of atoms on the hematite (001), (100), (110) and (012) facets; (c) XRD patterns of α-Fe_2O_3 NCs.

To further explore the crystalline structure of as-synthesized samples, XRD analysis was conducted. The sharp and narrow peaks of every sample in Fig. 2c corresponds to hexagonal hematite (α-Fe_2O_3, R-3c, JCPDS no. 33-0664). Additionally, the D-α-Fe_2O_3 NCs exhibited the highest intensity of (110) and (300) diffraction peaks, indicating better grown along the a- than the c- direction, resulting in plate and disk-like morphologies.[19] Generally, the final morphology of NCs was determined by the different growth rates of different planes, resulting in different gas sensing properties.

3.2. Gas sensing performance

Table 1 Comparison of formaldehyde-sensing properties of sensors based on different materials at room temperature.

Material	Structure	Con.(ppm)	Res.	T_{res}(s)	Ref.
Au-ZnO	octahedrons	800	2100	210	24
Au-ZnO	nanorod	100	6880	216	25
rGO-ZnO	flower particle	10	5.2	117	26
rGO-ZnO	nanorod	1	21	82	27
rGO-ZnO	quantum dot	100	210	30	28
rGO-ZnO	sheet	9	150	36	29
rGO-ZnO	flower particle	15	600	34	30
SnO_2-VG	sheet	5	550	46	31
NiS-Ni-ZnO	particle	10	330	39.4	32

ZnO-ANS-rGO	sheet	5	105	300	33
α-Fe_2O_3	spindle particle	1	6.5	<3	[This work]

Con.: Concentration; Res.: Response; T_{res}(s): Response time; Ref.: Reference

To investigate the gas sensing properties of the S-α-Fe_2O_3 NCs, the α-Fe_2O_3-deionized water dispersion was drop-coated onto an Al_2O_3 substrate (1.3 cm × 0.7 cm), as shown in Figure 3a and b. The current voltage (I-V) curve of the devices show a linear ohmic behavior between the sensing samples and the electrode (Fig. 3c).[20,21] In addition, the similar conductivity characteristics of three different devices indicated highly reproducibility. The responses of the S-α-Fe_2O_3 NCs-based sensor to HCHO (42) is remarkably higher than C_6H_7 and CH_3COCH_3, exhibiting a good selectivity (Fig. 3d). Chemical sensing experiments that conducted on target HCHO gases showed that all α-Fe_2O_3 NCs possessed n-type sensing behavior, and the current variation increased with decreasing proportion of (001) crystal plane (Fig. S1).[22,23] Surprisingly, the S-α-Fe_2O_3-based sensor showed rather fast response-recovery speed (<3 s) (Fig. 3e). Moreover, the response of the sensing layer could be tuned by HCHO gas concentrations. As a result, the S-α-Fe_2O_3 NCs-based sensor achieves a highly sensitive detection of 6.5-19 for 1-20 ppm HCHO (Fig. S2 and Fig. 3f). Compared with the reported sensors in the literature, the S-α-Fe_2O_3 NCs-based sensor stands out for HCHO sensing (Table 1).[24-33]

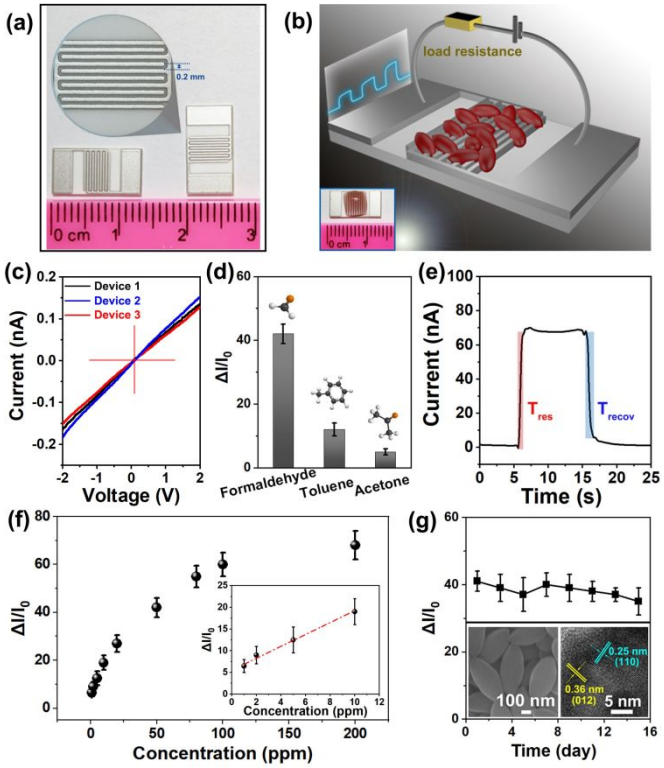

Fig. 3 (a) Optical images of the bare device with Pt interdigitated electrodes. (b) Schematic theoretical diagram of the gas sensor. (c) I-V curves of S-α-Fe_2O_3-based gas sensing devices. (d) selectivity of S-α-Fe_2O_3-based sensor towards 50 ppm formaldehyde, toluene and acetone. (e) Dynamic current curves of S-α-Fe_2O_3-based sensor against 100 ppm formaldehyde; (f) Response of the S-α-Fe_2O_3-based sensor vs HCHO concentration; (g) The responses of the S-α-Fe_2O_3-based sensor to 50 ppm HCHO during 15 days, and inset was the SEM and HRTEM images of S-α-Fe_2O_3 after 15 days.

To determine the practical feasibility of the sensor, the repeatability and long-term stability were evaluated. A consistent saturation behavior with no significant signal degradation was observed even after several repeated cycles, demonstrating the sustained response and recovery characteristics of the sensor (Fig. S3). Moreover, the sensor exhibited a long-term stability towards 50 ppm HCHO, as shown in Fig. 3g. It retained the morphology and sensing activity over the continuous 15-day test period.

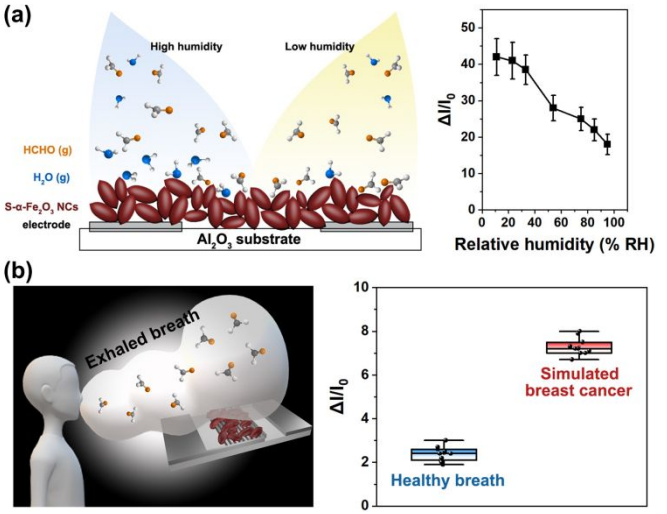

Fig. 4 (e) Relationship between the 50 ppm HCHO sensing response and relative humidity. (b) Simulated breath (breast cancer) sensing responses of S-α-Fe_2O_3-based sensor.

For real application, humidity should be considered as an important factor. As shown in Fig. 4a, a slight variation of sensing response occurred when RH below 40%, however, response approximately changed to half in high relative humidity, which could be explained as follows: (1) Water molecules blocked the adsorption of oxygen and HCHO gases; (2) Water molecules reacted with the adsorbed oxygen species, thus increasing the initial current baseline of the sensor; (3) OH groups from H_2O act as weak acceptors and compete with HCHO to occupy adsorption sites. Furthermore, to confirm the potential of the S-α-Fe_2O_3-based sensor for medical diagnosis, the sensor was exposed to the gas atmosphere of simulated breath of breast cancer (Fig. 4b). The fabricated S-α-Fe_2O_3-based sensor could discriminate the simulated breast cancer and healthy breath according to the response values with a large difference of about 4 times.

3.3. Gas sensing mechanism

α-Fe_2O_3 is a typical n-type MOS that electron is the carrier. The observed current variation was attributed to the reaction between the adsorbed oxygen species and the targets on the surface of α-Fe_2O_3 (Fig. 5a). When α-Fe_2O_3 exposed to air, the

electrons flowed from the conduction band of α-Fe_2O_3 to adsorbed oxygen, resulting in formation of negatively charged oxygen (O_2^-). Meanwhile, an electron depletion layer (space charge layer) created on the surface of α-Fe_2O_3. Thus, the resistance (current) of the α-Fe_2O_3-based sensor exhibited a high (low) baseline. After reducing gases (HCHO, C_7H_8, CH_3COCH_3) introduced, the electrons could be released back from gas molecules from gases. Thus, the resistance of the sensor decreased, that is, the current increased. Overall, the corresponding process could be simply expressed as follows:[34]

O_2 (gas) → O_2 (ads)

O_2 (ads) $+e^-$ → O_2^- (ads)

HCHO + O_2^- (ads) → CO_2 (gas)+ H_2O (gas) + e^-

$C_7H_8 + 9O_2^-$ → $4H_2O + 7CO_2 + 9e^-$

CH_3COCH_3 (gas) + $4O_2^-$ (ads) → $3CO_2$ (gas) + $3H_2O$ (gas) + $4e^-$

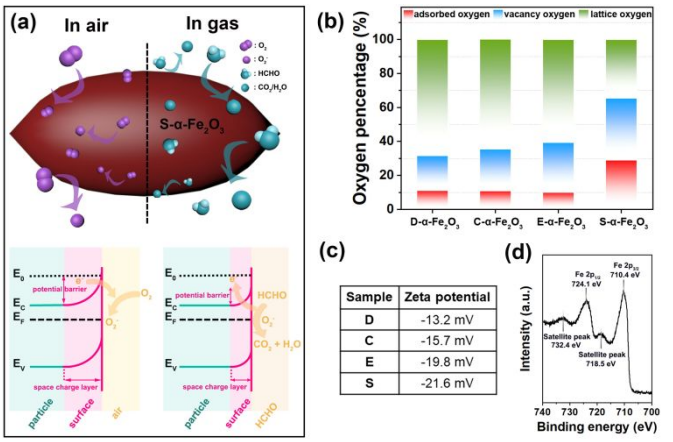

Sample	Zeta potential
D	-13.2 mV
C	-15.7 mV
E	-19.8 mV
S	-21.6 mV

Fig. 5 (a) Schematic model and energy band structure of the S-α-Fe_2O_3-based sensor in air and in HCHO. (b) The histogram of the percentage of chemisorbed oxygen and (c) the values of zeta potential of four α-Fe_2O_3 NCs. (d) Fe 2p XPS spectra of S-α-Fe_2O_3 NCs.

The adsorption capacity of the faceted α-Fe_2O_3 NCs could be characterized by their ability to adsorb oxygen. Thus, XPS analysis was carried out to explore the surface chemical states of existed elements on the α-Fe_2O_3 NCs. The O 1s spectra shown in Fig. S4 could be deconvoluted into three different oxygen species, namely lattice oxygen (O_L, ~530 eV), vacancy oxygen (O_V, ~531 eV) and the adsorbed oxygen (O_C, ~532 eV).[35] The O_L, O_V and O_C originated from to the O_2^- in the hematite lattice, the O_2^- around the oxygen vacancy regions in the matrix of hematite and the chemisorbed/dissociated oxygen species, respectively.[12] In Fig. 5b, S-α-Fe_2O_3 NCs showed the highest percentage of the O_C component among four samples. In addition, all samples showed negative zeta potential values, and the absolute value of S-α-Fe_2O_3 NCs is higher than those of other three samples, indicating that S-α-Fe_2O_3 NCs prefers to adsorb the ionized oxygen species with a more electrophilic surface layer (Fig. 5c). Furthermore, the strong binding energies at 724.1 and 710.4 eV were the characteristic doublets of Fe $2p_{1/2}$ and Fe $2p_{3/2}$, respectively (Fig. 5d). Besides, the appearance of satellite peaks at 718.5 and 732.4 eV confirmed the presence of ferric ions in α-Fe_2O_3.

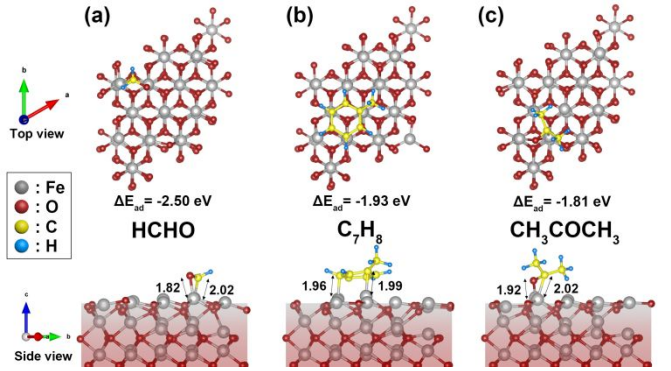

Fig. 6 Optimized adsorption geometries of the sensing process by DFT calculations for (a) HCHO, (b) C_7H_8, and (c) CH_3COCH_3.

To further explore the sensing mechanism and study the selectivity of S-α-Fe_2O_3 NCs-based sensors, DFT calculations were carried out. Three theoretical models combined with HCHO, C_7H_8, CH_3COCH_3 on the (001) surface of α-Fe_2O_3 were showed in Fig. 6.[21, 36] In comparison, the HCHO on the α-Fe_2O_3 has a shortest Fe-O bond length (1.82 Å), while the C_7H_8 and CH_3COCH_3 molecules yield Fe-C and Fe-O bond lengths (1.96 and 1.92 Å). Moreover, the adsorption energy of HCHO, C_7H_8 and CH_3COCH_3 molecules were -2.50 eV, -1.93 eV and -1.81 eV, respectively. The shortest bond length and largest adsorption energy on (001) faceted surface indicated the most stable adsorption configuration of HCHO gas, contributing to the adsorption and reaction between gas molecules and sensing materials.

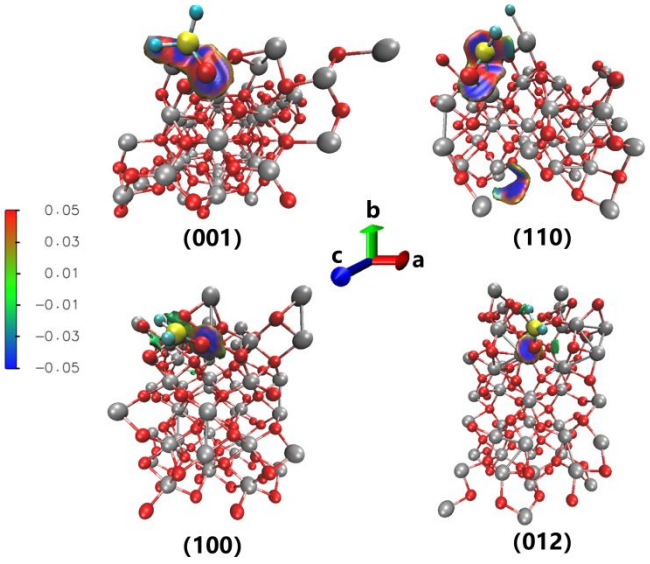

Fig. 7 Molecular structure map of HCHO adsorbed S-α-Fe_2O_3 with different exposed facets.

The numerous active sites for the adsorption of ionized oxygen species are attributed to the highly exposed reactive facets in α-Fe_2O_3 NCs.[37] In recent years, the powerful independent gradient model (IGM) method pose a visual analysis of intermolecular interactions. To gain more insight into the molecule surface adsorption, the facet effect of the α-

Fe_2O_3-based sensor was studied by IGM in the presence of HCHO, as shown in Fig. 7. The blue and red lobes represent prominent attractive interaction and repulsive interaction, respectively.[38] Compared with the other three facets, the attractive interaction between HCHO and (012) facet of α-Fe_2O_3 is more prominent, which explains why S-α-Fe_2O_3 exposed with high energy facets is more likely to interact with HCHO gas molecule. High-index facets may expose large numbers of unsaturated coordinated surface atoms, thus show modified electronic properties. Moreover, the high-index facets of α-Fe_2O_3 are conducive to the creation of lattice oxygen defects compared with the low-index facets, facilitating to the dissociative adsorption of reactant.[11] The above series of theory simulations highlights the advantages of using S-α-Fe_2O_3 with high energy facets on gas sensing.

Conclusions

In summary, a solvothermal method was conducted to synthesize α-Fe_2O_3 NCs for HCHO sensing. The morphology of α-Fe_2O_3 were successfully regulated through adjusting the volume ratio of EG to $NH_3 \cdot H_2O$. The S-α-Fe_2O_3 NCs was enclosed by a series of high-index facets, which exhibited excellent surface activity. Thus, the S-α-Fe_2O_3-based sensor exhibited superior HCHO sensing activity at room temperature with a response of 60 (100 ppm) and a fast response-recovery speed (<3 s). Furthermore, the healthy group and diseased group could be distinguished from each other, roughly through detecting the HCHO concentration in their exhaled breaths, indicating that the sensor exhibit the potential to assist physicians in diagnosis of breast cancer. According to the DFT results, the high selectivity of the sensor could be attributed to the short bond length and large adsorption energy on the (001), and the high sensitivity could be ascribed to the strong attractive reaction of HCHO on the (012) surface of α-Fe_2O_3. The facet engineering could be regarded as an efficient strategy for the gas device design.

Acknowledgements

This work was supported by the National Natural Science Foundation of China (NSFC; Grant No. 22106015, 62101093).

Notes and references

1 M. S. Niu, H. H. Yang, H. Zhou, X. L. Yi, X. Zhou, J. J. Zhan, Y. Liu, *Chem. Eng. J.* 2022, **431**, 133928.
2 K. C. Wan, D. Wang, F. Wang, H. J. Li, J. C. Xu, X. Y. Wang, J. H. Yang, *ACS Appl. Mater. Interfaces* 2019, **11**, 45214-45225.
3 Y. Zheng, J. Wang, P. Yao, *Sens. Actuators B* 2011, **156**, 723-730.
4 W. Liu, J. Sun, L. Xu, S. D. Zhu, X. Y. Zhou, S. Yang, B. Dong, X. Bai, G. Y. Lu, H. W. Song, *Nanoscale Horiz.* 2019, **4**, 1361-1371.
5 R. Zhang, S. Cao, T. T. Zhou, T. Fei, R. Wang, T. Zhang, *Sens. Actuators B* 2020, **310**, 127695.
6 Z. Yang, W. Y. Cao, C. H. Peng, T. Wang, B. L. Li, H. L. Ma, Y. J. Su, Z. H. Zhou, J. H. Yang, M. Zeng, *IEEE Sens. J.* 2021, **9**, 11023-11030.
7 A. Shanmugasundaram, S. V. Manorama, D. S. Kim, Y. J. Jeong, D. W. Lee, *Chem. Eng. J.* 2012, **448**, 137736.
8 D. Mao, J. Yao, X. Lai, M. Yang, J. Du, D. Wang, *Small* 2011, **7**, 578-582.
9 W. C. Geng, S. B. Ge, X. W. He, S. Zhang, J. W. Gu, X. Y. Lai, H. Wang, Q. Y. Zhang, *ACS Appl. Mater. Interfaces* 2018, **10**, 13702-13711.
10 Y. F. Li, P. Zhang, J. Xiong, Y. C. Wei, H. J. Chi, Y. L. Zhang, K. Z. Lai, Z. Zhao, J. G. Deng, *Environ. Sci. Technol.* 2021, **55**, 16153−16162.
11 M. H. Chen, H. Yin, X. Y. Li, Y. P. Qiu, G. X. Cao, J. J. Wang, X. F. Yang, P. Wang, *J. Hazard. Mater.* 2020, **395**, 122628.
12 J. Zhao, P. Yang, H. S. Chen, J. Li, Q. D. Che, Y. N. Zhu, R. X. Shi, *J. Mater. Chem. C* 2015, **3**, 2539-2547.
13 H. T. Fan, Y. Zeng, H. B. Yang, X. J. Zheng, L. Liu, T. Zhang, *Acta Phys.-Chim. Sin.* 2008, **24**, 1292-1296.
14 R. Zhang, J. W. Shi, T. T. Zhou, J. C. Tu, T. Zhang, *J. Colloid Interf. Sci.* 2019, **539**, 490-496.
15 J. X. Dai, X. Guan, H. R. Zhao, S. Liu, T. Fei, T. Zhang, *Sens. Actuators B* 2020, **367**, 132134.
16 V. J. Vande, J. Hutter, *J. Chem. Phys.* 2007, **127**, 114105.
17 Y. H. Gui, K. Tian, J. X. Liu, L. L. Yang, H. Z. Zhang, Y. Wang, *J. Hazard. Mater.* 2019, **380**, 120876.
18 A. R. Chen, L. Xu, X. J. Zhang, Z. M. Yang, S. C. Yang, *ACS Appl. Mater. Interfaces* 2016, **8**, 33765-33774.
19 L. Chen, X. Yang, J. Chen, J. Liu, H. Wu, H. Zhan, C. Liang, M. Wu, *Inorg. Chem.* 2010, **49**, 8411-8420.
20 Z. L. Wu, Z. J. Li, H. Li, M. X. Sun, S. B. Han, C. Cai, W.Z . Shen, Y. Q. Fu, *ACS Appl. Mater. Interfaces* 2019, **11**, 12761-12769.
21 L. L. Wang, R. Q .Chai, Z. Lou, G. Z. Shen, *Nano Res.* 2018, **11**, 1029-1037.
22 Q. Ye, C. Y. Liu, J. N. Li, H. Y. Wang, S. H. Yan, M. Y. Meng, H. Y. Xu, *Sens. Actuators B* 2022, **367**, 132134.
23 H. Fu, H. Y. Shao, L. W. Wang, H. Jin, D. H. Xia, S. W. Deng, Y. H. Wang, Y. Chen, C. Z. Hua, L. Liu, L. Zang, *ACS Sens.* 2020, **5**, 571-579.
24 Y. Li, H. Jin, G. Sun, B. Zhang, N. Luo, L. Lin, H. Bala, J. Cao, Z. Zhang, Y. Wang, *Phys. E Low Dimens. Syst. Nanostruct.* 2019, **106**, 40-44.
25 J. Huang, H. Liang, J. Ye, D. Jiang, Y. Sun, X. Li, Y. Geng, J. Wang, Z. Qian, Y. Du, *Sens. Actuators B* 2021, **346**, 130568.
26 X. Li, J. Wang, D. Xie, J. Xu, R. Dai, L. Xiang, H. Zhu, Y. Jiang, *Sens. Actuators B* 2015, **221**, 1290-1298.
27 N. Minh Triet, L. Thai Duy, B. U. Hwang, A. Hanif, S. Siddiqui, K. H. Park, C. Y. Cho, N. E. Lee, *ACS Appl. Mater. Interfaces* 2017, **9**, 30722-30732.
28 Q. Huang, D. Zeng, H. Li, C. Xie, *Nanoscale* 2012, **4**, 5651-5658.
29 H. Mu, Z. Zhang, X. Zhao, F. Liu, K. Wang, H. Xie, *Appl. Phys. Lett.* 2014, **105**, 033107-033112.
30 X. Li, J. Wang, D. Xie, J. Xu, R. Dai, L. Xiang, H. Zhu, Y. Jiang, *Sens. Actuators B* 2015, **221**, 1290-1298.
31 Z. Bo, M. Yuan, S. Mao, X. Chen, J. Yan, K. Cen, *Sens. Actuators B* 2018, **256**, 1011-1020.
32 Y. Z. Yang, S. N. Wu, Y. H. Cao, S. Li, T. F. Xie, Y. H. Lin, Z. H. Li, *J. Alloys Compd.* 2022, **920**, 165850.
33 J. Fan, H. Li, H. Hu, Y. Niu, R. Hao, A. Umar, M. S. Al-Assiri, M. A. Alsaiari, Y. Wang, *Microchem. J.* 2021, **160**, 105607.
34 M. N. Ding, D. C. Sorescu, A. Star, *J. Am. Chem. Soc.* 2013, **135**, 9015-9022.
35 H. J. Song, S. W. Yan, Y. L. Yao, L. X. Xia, X. L. Jia, J. S. Xu, *Chem. Eng. J.* 2019, **370**, 1331-1340.
36 C. Gao, Q. Q. Meng, K. Zhao, H. J. Yin, D. W. Wang, J. Guo, S. L. Zhao, L. Chang, M. He, Q. X. Li, *Adv. Mater.* 2016, **28**, 6485-6490.

37 M. H. Chen, H. Yin, X. Y. Li, Y. P. Qiu, G. X. Cao, J. J. Wang, X. F. Yang, P. Wang, *J. Hazard. Mater.* 2020, **395**, 122628.
38 T. Lu, Q. X. Chen, *J Comput. Chem.* 2022, **43**, 539-555.

Graphical Abstract

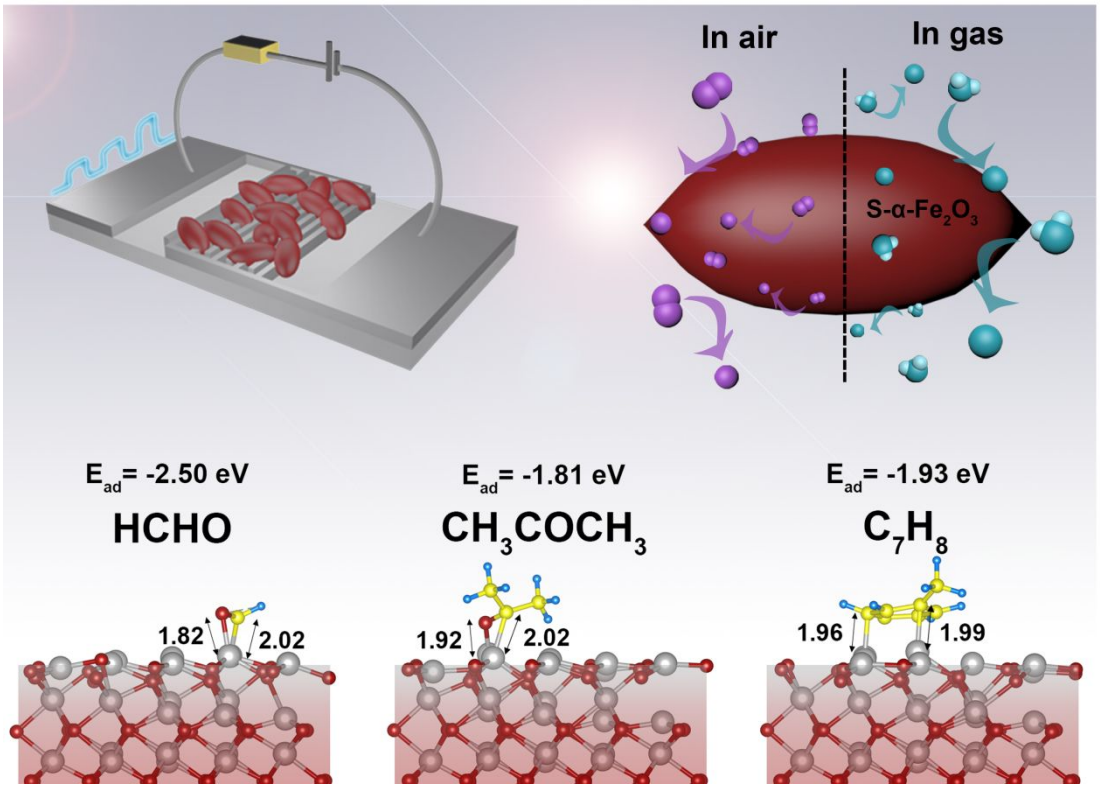

Electronic Supplementary Information (ESI)

For

Room-temperature formaldehyde sensor based on hematite for breast cancer diagnosis

Rui Zhang[1], Chuanqun Liu[1], Pu Wang[1], Yang Li[3], Yue Su[4], Jianxun Dai*[2]

1. School of Environmental Science and Technology, Key Laboratory of Industrial Ecology and Environmental Engineering (Ministry of Education), Dalian University of Technology, Dalian, 116024, China

2. School of Optoelectronic Engineering and Instrumentation Science, Dalian University of Technology, Dalian, 116024, China.

3. Department of Electronic Systems, Norwegian University of Science and Technology, NO-7491, Trondheim, Norway.

4. Institute of Semiconductors, Chinese Academy of Sciences, Beijing, 100864, China.

Email: jianxundai@dlut.edu.cn

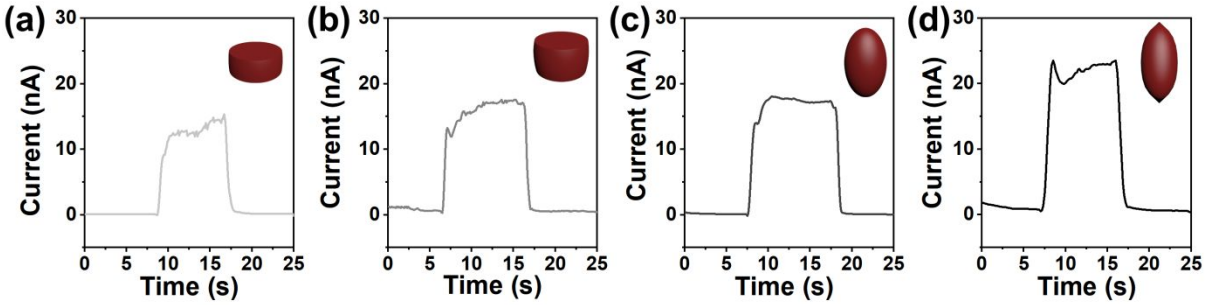

Figure S1. Response-recovery curve of four α-Fe_2O_3 NCs-based sensors to 20 ppm HCHO.

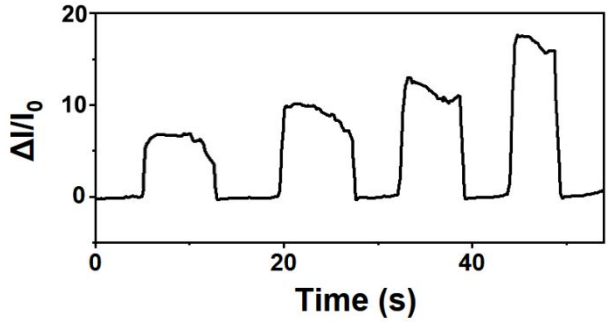

Figure S2. Response-recovery curve of the S-α-Fe_2O_3 NCs-based sensor to 1-20 ppm HCHO.

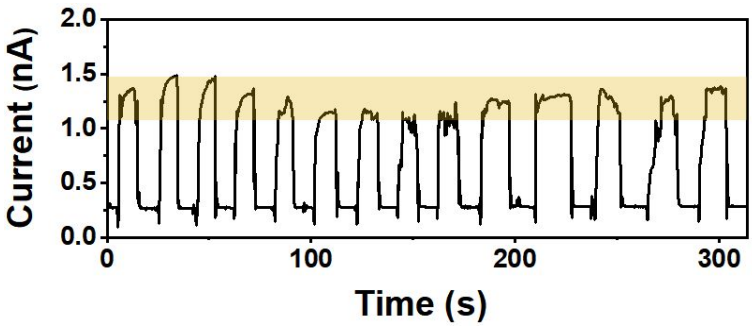

Figure S3. Response-recovery curve of S-α-Fe_2O_3 NCs-based sensor to 0.5 ppm HCHO.

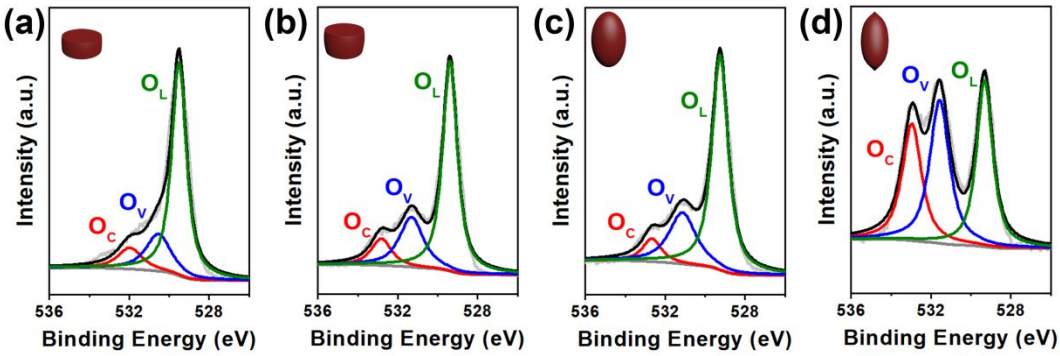

Figure S4. O 1s high-resolution spectra of four α-Fe_2O_3 NCs.

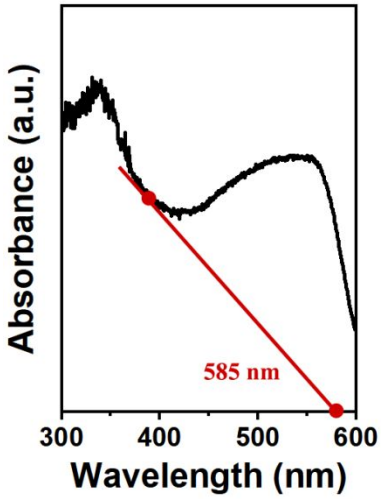

Figure S5. The UV-visible absorption spectrum of S-α-Fe_2O_3 NCs.

The calculated band gap of S-α-Fe_2O_3 NCs is about (1240/585=) 2.12 eV, which confirmed the wide band-gap property and corresponded to the previous reports.[1-2]

References:

[1] K. E. Krafft, C. Wang, W. B. Lin, *Adv. Mater.* 2012, **24**, 2014-2018.

[2] S. Huang, T. Ouyang, B. F. Zheng,M. Dan, Z. Q. Liu, *Angew. Chem. Int. Ed.* 2021, **133**, 9632-9638.